

# Gamma spectrometry for chronology of recent sediments

## *Tracing human induced climate change in NW Africa*

D. Pittauerová<sup>a</sup>, S. Mulitza<sup>b</sup>, H.W. Fischer<sup>a</sup>

<sup>a</sup> Institute of Environmental Physics,  
University of Bremen,  
Bremen, Germany

<sup>b</sup> MARUM - Center for Marine Environmental Sciences,  
University of Bremen,  
Bremen, Germany

**Abstract.** Gamma spectroscopy was used for determination of radionuclides in sediment cores from the continental shelf off NW Africa to provide age control of the sediment record used for a study of aridification of the Sahel zone.  $^{210}\text{Pb}$ ,  $^{226}\text{Ra}$  and  $^{137}\text{Cs}$  were measured in the upper part of a gravity core and the associated multicorer and used for aligning these cores. This provided information about the amount of sediment loss due to the sampling procedure in the upper part of the gravity core. The age model based on the matched profiles extended to 140 years B.P. and the rest of the gravity core was dated by  $^{14}\text{C}$ . The  $^{210}\text{Pb}$  age allowed the estimation of the local radiocarbon reservoir age. Application of  $^{210}\text{Pb}$  and  $^{137}\text{Cs}$  chronology helps significantly to extend paleoclimatic proxy data into the Anthropocene, thereby allowing to compare human induced climate change with natural climate variability.

## 1. Introduction

Gamma spectroscopy is a widely used method for studying sediment samples. A number of radioisotopes which can be used for dating young sediment sequences or tracing changes in recent parts of sediment cores, are routinely analyzed. These include most often:

- U/Th decay series members:  $^{210}\text{Pb}$ ,  $^{226}\text{Ra}$  (via  $^{214}\text{Pb}$  and  $^{214}\text{Bi}$ ),  $^{234}\text{Th}$ ,  $^{228}\text{Th}$  (via  $^{212}\text{Pb}$ ,  $^{212}\text{Bi}$  and  $^{208}\text{Tl}$ ),  $^{228}\text{Ra}$  (via  $^{228}\text{Ac}$ )
- Primordial isotope:  $^{40}\text{K}$
- Cosmogenic isotope:  $^7\text{Be}$
- Artificial isotopes:  $^{137}\text{Cs}$ ,  $^{241}\text{Am}$ .

$^{210}\text{Pb}$  (half-life 22.3 years) is a part of  $^{238}\text{U}$  series. It enables relative dating of ages between 20-150 years and is used for estimation of sedimentation rates in lakes, estuaries and marine sediments as part of environmental, pollution and climate change studies [1].  $^{210}\text{Pb}$  in sediments consists of two components: supported  $^{210}\text{Pb}$  ( $^{210}\text{Pb}_{\text{sup}}$ ), which is present due to autigenic material of the sediment and is usually assumed to be in radioactive equilibrium with its parent nuclide  $^{226}\text{Ra}$  (half-live 1600 yr) and unsupported (or excess)  $^{210}\text{Pb}$  ( $^{210}\text{Pb}_{\text{xs}}$ ), which originates from the atmospheric deposition. Unsupported lead is then determined by subtracting supported activity from the total activity and used for estimation of accumulation rates and age models.

Measurement techniques of total signal of  $^{210}\text{Pb}$  ( $^{210}\text{Pb}_{\text{tot}}$ ) include alpha spectroscopy via  $^{210}\text{Po}$  with assumption of radioactive equilibrium between  $^{210}\text{Po}$  and  $^{210}\text{Pb}$ , or gamma spectroscopy. Advantages of gamma spectroscopy over alpha spectroscopy of  $^{210}\text{Pb}$  [2], are that gamma spectroscopy is non-destructive, several isotopes can be measured simultaneously in one spectrum (including  $^{210}\text{Pb}_{\text{sup}}$ ), only physical preparation of the samples (no time consuming chemical separation) is needed and the

detection efficiency is only dependent on physical parameters. On the other hand, this method has certain disadvantages. It requires large amount of sample (minimum 1 g d.m., optimum about 50 g d.m.) for the analysis, gamma spectra have higher and more complicated background, detection efficiency varies with gamma energy and self-absorption of gamma radiation in the sample itself must be considered.

$^{137}\text{Cs}$ , an artificial radionuclide introduced to the atmosphere by nuclear bomb-tests, nuclear accidents and routine discharges from nuclear installations, has a half-life of 30 years. It is often used as a complementary independent and also an absolute chronometer for the last 60 years. Its onset in the environment can be observed since early 1950's, with maximum nuclear test fallout occurring in 1963. In Europe, 1986 Chernobyl accident represents another important input of  $^{137}\text{Cs}$ .

## 2. Methods

### 2.1. Sampling

Terrigenous sediments deposited at marine site GeoB9501 were sampled by high resolution gravity core (GC) GeoB9501-5 (16°50.44'N, 16°43.97'W, 323 m depth) and multicore (MUC) GeoB9501-4 (16°50.38'N, 16°43.96'W, 330 m depth) on the northern rim of the Mauretania Canyon in Senegal Mud Belt, during the METEOR Cruise M65/1 in June 2005 (Fig. 1). A multicorer deployed to recover sediment-water interface, the undisturbed sediment surface to the depth of 42 cm and the overlying water, was equipped with 8 large and 4 small plastic tubes, each of 60 cm length and 10 and 6 cm in diameter, respectively. A core recovered using one of the larger tubes was used for radiometric analysis. A gravity corer was deployed to recover longer sediment sequences of total 532 cm. This set of cores was used as a sediment archive for interpreting 3200 year history of Sahel droughts [3].

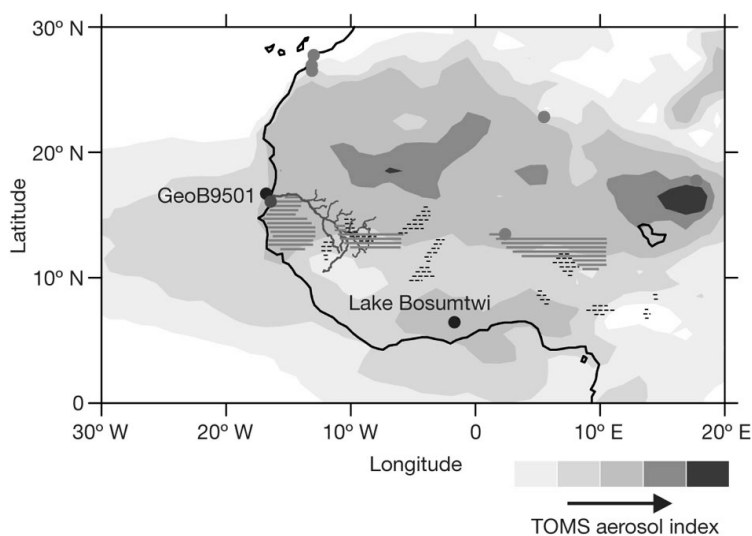


**FIG. 1.** Location of the marine site GeoB9501 (from [3]). The averaged TOMS 1997-2005 aerosol (<http://toms.gsfc.nasa.gov/>) shows the Sahara-Sahel dust corridor. Aeolian dust together with Senegal river suspension is the main constituent of the GeoB9501 sediment. Horizontal hatching indicates agricultural areas with groundnut (solid) and cotton (dashed) production in AD 1914.

### 2.2. Samples preparation

Material of each 1 cm slice of MUC and every other 1 cm slice of GC (upper 42 cm long part of the core – 21 slices) was placed in the wet form into cylindrical plastic containers with diameter of 69 mm and height 20 mm. The MUC samples (total 42 slices) were filled in variable heights in the measurement dishes in order to use maximal amount of the material, while the GC samples were filled

to a uniform height of 10 mm. All measurement dishes were sealed in radon proof foil for a minimum of 3 weeks to establish radioactive equilibrium between  $^{226}\text{Ra}$  and  $^{222}\text{Rn}$  (and its daughter products).

### 2.3. Gamma spectroscopy

The samples of both GC and MUC were analyzed by low-level low-background gamma spectroscopy using a coaxial HPGe detector (Canberra Industries) of 50% rel. efficiency housed in a 10 cm Pb shielding with Cu, Cd and plastic lining, operated under Canberra Genie 2000 software. Activity concentrations in  $\text{Bq}\cdot\text{kg}^{-1}$  in wet mass sediment of  $^{210}\text{Pb}$ ,  $^{137}\text{Cs}$ ,  $^{214}\text{Bi}$ ,  $^{214}\text{Pb}$  and  $^{40}\text{K}$  were determined. Activity concentrations in  $\text{Bq}\cdot\text{cm}^{-3}$  were calculated by multiplying with measured wet densities for MUC. For GC, sediment volume could not be estimated reliably, therefore activity concentrations in  $\text{Bq}\cdot\text{kg}^{-1}$  dry mass were used instead. The latter quantity was also used for aligning of MUC and GC profiles.

$^{210}\text{Pb}_{\text{xs}}$  activity concentrations were calculated for each sample as a difference between  $^{210}\text{Pb}_{\text{tot}}$  and  $^{210}\text{Pb}_{\text{sup}}$ . For estimation of  $^{210}\text{Pb}_{\text{sup}}$ ,  $^{214}\text{Pb}$  in equilibrium with  $^{226}\text{Ra}$  was used. Additionally, self attenuation corrections for low-energy  $^{210}\text{Pb}$  (45.6 keV,  $I_{\gamma}$  4.25%) for the MUC were necessary due to varying sample geometries. They were calculated using a modification of Hurtado et al. 2007 method [4], combining both experimental transmission measurements and mathematical Monte Carlo simulations. In this study, the full-energy peak efficiencies for samples of zero density with different heights in measurement containers were generated using the Monte Carlo based LabSOCS Genie 2000 calibration tool [5]. For the associated GC no individual self-attenuation corrections were applied for  $^{210}\text{Pb}$  due to constant geometry of the samples. Instead, efficiency values experimentally obtained with test sources of similar geometry were used.

## 3. Results and discussion

### 3.1. $^{210}\text{Pb}_{\text{xs}}$ and $^{137}\text{Cs}$ age model

The age model for MUC and GC was developed using a combination of two independent radiometric methods.  $^{210}\text{Pb}_{\text{xs}}$  and  $^{137}\text{Cs}$  pair was employed for the upper part of the cores and AMS radiocarbon dating of planktonic foraminifera for the rest of the GC [3].

For  $^{210}\text{Pb}_{\text{xs}}$  age model of MUC, the classical constant rate of supply (CRS) model was applied [6]. The absolute chronology extends to AD 1915 $\pm$ 7 in the depth of 42.5 cm.  $^{137}\text{Cs}$  activity concentrations were compared to the expected  $^{137}\text{Cs}$  bomb fallout atmospheric input. The  $^{137}\text{Cs}$  data show a broad maximum in approximately AD 1962–81. The onset of  $^{137}\text{Cs}$  in the profile in AD 1947 $\pm$ 3 is in a relatively good agreement with atmospheric bomb testing initiation in early 1950's. Due to rather low  $^{137}\text{Cs}$  values, the measurement uncertainties are high and do not provide fine resolution. It was not possible to clearly identify the AD 1963 nuclear fallout peak or contribution of the geographically close 4 Algerian atmospheric tests, performed in AD 1960–61. Nevertheless, the shape of the  $^{137}\text{Cs}$  profile is compatible with the bomb fallout chronology, possibly followed by a terrestrial erosion component, especially when the activities are decay corrected using ages derived from  $^{210}\text{Pb}_{\text{xs}}$  chronology (Fig. 2).

### 3.2. Matching the cores and extending the chronology

During sampling using a gravity corer, usually some loss of material on the top of core is inevitable. It is thus important to determine, how much material was lost during sampling procedure. Obtaining a continuous profile by aligning GC and MUC is also desirable. Routinely this is done by colour, physical properties, stable isotopes or main elements content. Our approach suggests using radionuclide data for matching MUC and GC.

Depth aligning of the GC and the MUC was performed using the corresponding  $^{210}\text{Pb}_{\text{xs}}$  and  $^{137}\text{Cs}$  profiles using method based on least square fitting described in [7]. The onset of  $^{137}\text{Cs}$  corresponds to a depth of 29.5 cm in MUC and to a depth of 8 cm GC. About 21.5 cm long upper segment of sediment

material was lost during gravity coring (Fig. 2). The correctness of the matching was independently validated by profiles of the main element composition (Al, Si, K, Fe, Ti) and their ratios, which were also variable [7]. The  $^{210}\text{Pb}_{\text{xs}}$  profile appears to be disturbed in the uppermost part of the GC (not an unusual finding due to the mechanical impact applied during the coring procedure), but it shows a very good continuity to the MUC-B profile from the composite depth of 43 cm downwards, which enables extension of the chronology.

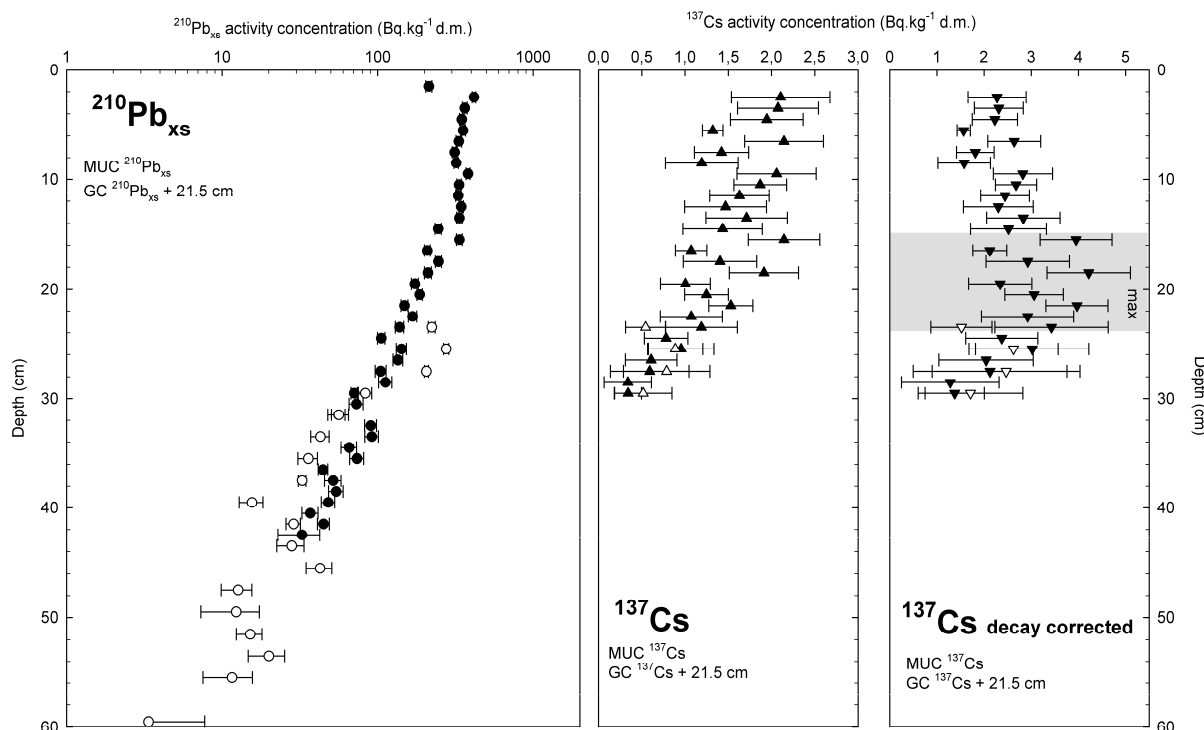


FIG. 2. Depth matching of the MUC and GC records for  $^{210}\text{Pb}_{\text{xs}}$  (log-scale, left) and  $^{137}\text{Cs}$  (linear scale, middle and right) profiles. The error bars for all data are 1 standard deviation (they include counting statistics and calibration of the measuring device).  $^{137}\text{Cs}$  under 30 cm depth are below detection limit.  $^{137}\text{Cs}$  profile in the right is decay corrected to the date of analysis using ages derived from  $^{210}\text{Pb}_{\text{xs}}$  model. A broad maximum in approximately AD 1962–81 is shaded.

Following the aligning of MUC and GC, the age model for the MUC could be extended to the GC based on an average sedimentation rate obtained from a combined record of MUC  $^{210}\text{Pb}_{\text{xs}}$  data from the depths of 16.5–42.5 cm with the follow-up part of the GC (depth 43.5–63.5 cm) (Fig. 3). This part of the composite profile showed exponential decrease, which enabled to express a mean sedimentation rate based on an exponential fit obtained by the least squares method. The average sedimentation rate was then used for dating the upper part of the GC to the composite depth of 63.5 cm, corresponding to AD 1864±9.

The combined MUC and GC chronology based on gamma spectroscopy covered the youngest 140 years old part of the core. The interconnection of the combined  $^{210}\text{Pb}_{\text{xs}}$  and  $^{137}\text{Cs}$  model to the radiocarbon model of the GC (Fig. 3) was constructed by fitting a weighted four-order polynomial function to the pooled  $^{210}\text{Pb}_{\text{xs}}$  and calibrated radiocarbon ages by least square method [3].

### 3.3. Radiocarbon reservoir age

The  $^{210}\text{Pb}_{\text{xs}}$  age model allowed the estimation of the local radiocarbon reservoir age using the AMS  $^{14}\text{C}$ -date of a foraminifera sample from the bottom of a parallel core (45.5 cm) from the same MUC cast. From the  $^{210}\text{Pb}_{\text{xs}}$ -based age model, it was estimated that this core depth corresponds to AD 1907.

The calculated local reservoir effect of 140 years [3] was used for calibration of the conventional AMS radiocarbon dates of GC. A constant reservoir age was assumed throughout the time period covered by the sediment record.

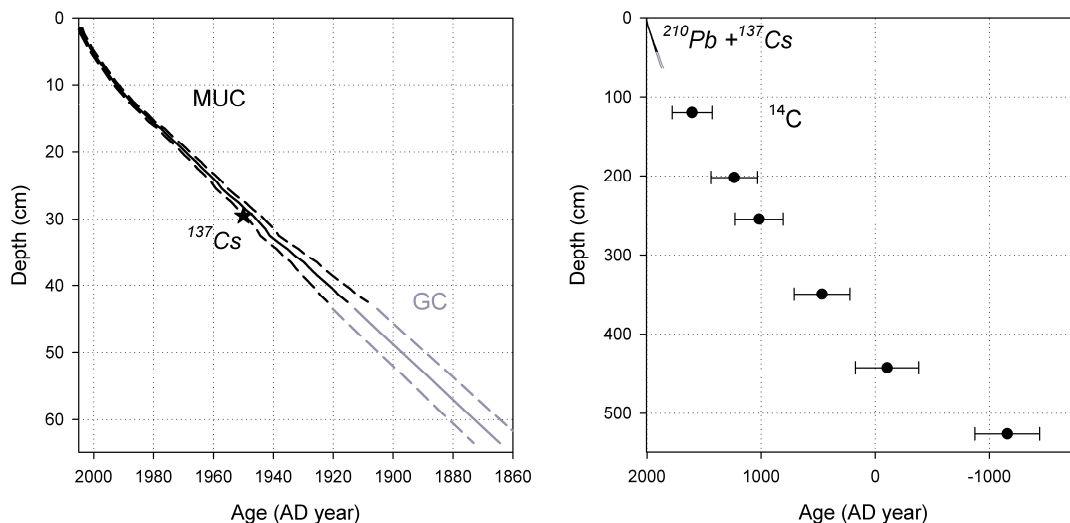


FIG. 3. Left: Extended  $^{210}\text{Pb}_{\text{xs}}$  chronology for aligned MUC and GC. The dashed lines stand for  $1\sigma$  confidence limit of  $^{210}\text{Pb}_{\text{xs}}$  age.  $^{137}\text{Cs}$  onset in the depth of 29.5 cm is in a good agreement with  $^{210}\text{Pb}_{\text{xs}}$  chronology. Right: Radiocarbon ages [3] (error bars indicating 2 standard deviations) together with  $^{210}\text{Pb}_{\text{xs}}$  chronology from the left figure.

### 3.4. Use of the age model for paleoclimatological interpretations

Further sediment sample parameters were determined, including bulk geochemistry of Si, Al, Ti, K, Ca and grain size analysis was performed by team of MARUM. The data were analyzed and interpreted in Mulitza et al. [3]. The main constituents of the studied sediment material are aeolian dust (Si rich, with particles up to 200  $\mu\text{m}$ ) and fine Senegal river suspension (Al and Fe rich, 95% < 10  $\mu\text{m}$ ). The relative proportions of riverine, aeolian and marine contributions were evaluated by end-member analysis. Dust and fluvial end-members were constructed using the normalized relative abundances of Si, Al, Ti, K and Ca from modern aeolian and riverborne materials and the marine end-member was constructed theoretically (98% Ca, 2% Si) [3]. Knowing sedimentation rates enabled to express dust fluxes in the past (Fig. 4).

The reconstruction of the history of the African dust generation showed, that the onset of commercial agriculture about 200 years ago started to contribute to the overall dust budget (Fig. 4). Corn was introduced to the Sahel in early 18<sup>th</sup> Century. It was gradually replaced by millet and sorghum in the mid 18<sup>th</sup> Century. The steepest dust deposition increase can be observed in the period of commercial peanuts production in Senegal, Nigeria and Gambia starting with 1840s. It was suggested, that deforestation and expansion of agriculture use of the land in Sahel zone contributed extensively to wind erosion in the region [3].

### ACKNOWLEDGEMENTS

The authors would like to thank to W. Chehade (Institute of Environmental Physics, University of Bremen) for assistance in measuring and analyzing the samples by gamma spectroscopy. Combining the  $^{210}\text{Pb}_{\text{xs}}$  based model with radiocarbon and calculation of local radiocarbon reservoir age was performed by G. Mollenhauer (MARUM, University of Bremen).

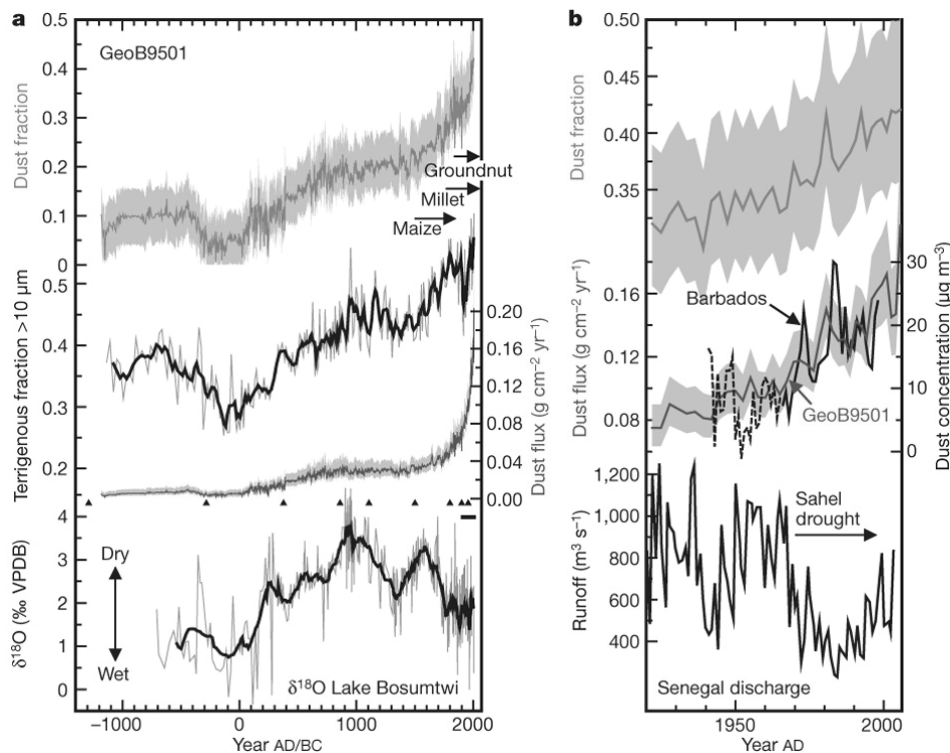


FIG. 4. Left (from [3]): The mean dust fraction, terrigenous grain-size fraction  $> 10 \mu\text{m}$  and dust deposition flux records were compared to literature data on  $\Delta^{18}\text{O}$  authigenic carbonate from the lake Bosumtwi(Ghana), indicating dry and wet periods in Sahel history. The triangles indicate radiocarbon age control and the horizontal bar the time period dated by  $^{210}\text{Pb}_{\text{xs}}$  and  $^{137}\text{Cs}$  method.

Right (from [3]): Recent records of mean dust fraction and dust deposition flux compared to instrumental measurements of airborne African dust concentrations at Barbados from mid-1960s (the pre-1968 record is estimated from regression with Sahel precipitation) and Senegal river discharge.

## REFERENCES

- [1] APPLEBY, P.G., Three decades of dating recent sediments by fallout radionuclides: a review, *Holocene* **18** (2008) 83.
- [2] ZABORSKA, A., CARROLL, J., PAPUCCI, C., PEMPKOWIAK, J., Intercomparison of alpha and gamma spectrometry techniques used in  $^{210}\text{Pb}$  geochronology. *J. Env. Rad.* **93** (2007) 38 – 50.
- [3] MULITZA, S., HESLOP, D., PITTAUEROVÁ, D., FISCHER, H.W., ZABEL, M., MOLLENHAUER, G., COLLINS, J.A., KUHNERT, H., STUUT, J-B., SCHULZ, M., Intensification of African dust emissions with the onset of commercial agriculture in the Sahel Region, *Nature* **244** (2010) 226.
- [4] HURTADO, S., VILLA, M., MANJÓN, G., GARCÍA-TENORINO, R., A self-sufficient and general method for self-absorption correction in gamma-ray spectrometry using GEANT4, *Nucl. Instrum. Meth. A* **580** 1 (2007) 234-237.
- [5] BRONSON, F.L., Validation of the accuracy of the LabSOCS software for mathematical efficiency calibration of Ge detectors for typical laboratory samples. *J. Radioanal. Nucl. Ch.* **255** 1 (2003) 137-141.
- [6] APPLEBY, P.G., OLDFIELD, F., The calculation of lead-210 dates assuming a constant rate of supply of unsupported  $^{210}\text{Pb}$  to the sediment. *Catena* **5** (1978) 1-8.
- [7] PITTAUEROVÁ, D., FISCHER, H.W., MULITZA, S. “Using  $^{210}\text{Pb}$  and  $^{137}\text{Cs}$  record for matching sediment cores”. Proc. International Topical Conference on Polonium and Radioactive Lead Isotopes, Seville, Spain, October 2009.